Chinese Chemical Letters 36 (2025) 110293

Contents lists available at ScienceDirect

Chinese Chemical Letters

journal homepage: www.elsevier.com/locate/cclet

New insights into electrocatalytic singlet oxygen generation for effective and selective water decontamination

Shengtao Jiang[a], Mengjiao Xie[b], Limin Jin[b], Yifan Ren[b], Wentian Zheng[b], Siping Ji[c,*], Yanbiao Liu[b,*]

[a] Zhejiang Provincial Key Laboratory of Plant Evolutionary Ecology and Onservation, School of Life Science, Taizhou University, Taizhou 318000, China
[b] College of Environmental Science and Engineering, Donghua University, Shanghai 201620, China
[c] School of Chemistry Science and Engineering, Yunnan University, Kunming 650091, China

ARTICLE INFO

Article history:
Received 21 April 2024
Revised 1 July 2024
Accepted 23 July 2024
Available online 25 July 2024

Keywords:
CoFe alloy
Oxygen activation
Singlet oxygen
Electrocatalytic system water decontamination

ABSTRACT

Singlet oxygen ($^1O_2$), as an electrophilic oxidant, is essential for the selective water decontamination of pollutants from water. Herein, we showcase a high-performing electrocatalytic filtration system composed of carbon nanotubes functionalized with CoFe alloy nanoparticles (CoFeCNT) to selectively facilitate the electrochemical activation of O_2 to $^1O_2$. Benefiting from the prominently featured bimetal active sites of CoFeCNT, nearly complete production of $^1O_2$ is achieved by the electrocatalytic activation of O_2. Additionally, the proposed system exhibits a consistent pollutant removal efficiency >90% in a flow-through reactor over 48 h of continuous operation without a noticeable decline in performance, highlighting the dependable stability of the system for practical applications. The flow-through configuration demonstrates a striking 8-fold enhancement in tetracycline oxidation compared to a conventional batch reactor. This work provides a molecular level understanding of the oxygen reduction reaction, showing promising potential for the selective removal of emerging organic contaminants from water.

Recently, the effective and selective removal of emerging organic contaminants (EOCs) has drawn significant attention [1-4]. A notable surge in the advancement of molecular oxygen (O_2) activation technology has drawn considerable interest within the realm of advanced oxidation processes (AOPs). This innovative approach can generate a variety of reactive oxygen species (ROS) [5], including free radicals (*e.g.*, hydroxyl radicals (•OH) and sulfate radicals) and non-radical species such as singlet oxygen ($^1O_2$). $^1O_2$ is a highly reactive non-radical ROS that offers a selective ability to oxidize ($E_0(^1O_2/H_2O) = 2.17$ V *vs.* NHE) electron-rich micropollutants (ng/L to μg/L) as well as a high tolerance to environmental factors that could interfere with oxidation [6-8]. The primary techniques for producing $^1O_2$ in AOPs rely on the utilization of hydrogen peroxide (H_2O_2) and peroxymonosulfate [9,10]. Nevertheless, their practical utility is limited by their need for external chemical inputs, intrinsic limits in activation selectivity and inadequate ability to degrade micropollutants [11]. Hence, advanced strategies for the direct synthesis of $^1O_2$ from ground state O_2 are highly desirable.

The formation of $^1O_2$ is linked to the "end-on" adsorption configuration of O_2 on the metal active sites, promoting the cleavage of an M–O bond instead of an O–O bond, which also plays a pivotal role in fostering the formation of –O–O– intermediates (critical intermediates for $^1O_2$) [12,13]. The "end-on" adsorption O_2 to metal sites significantly increases the likelihood of $^1O_2$ production by enabling the reduction or disproportionate reaction of –O–O– intermediates [14-16]. Consequently, these problems may be addressed by formulating innovative approaches to enhance the efficacy of the transformation of *OOH into $^1O_2$ [17-19].

To this end, catalysts based on Prussian blue analogues (PBAs) that contain transition metal cations and CN^- groups have been extensively pursued for the oxygen reduction reaction (ORR) because of their adjustable composition and exceptional electrochemical properties [20-23]. A crucial challenge regarding the synthesis of PBA-derived catalyst is their irreversible agglomeration and collapse. Fortunately, one-dimensional carbon nanotubes (CNT) with exceptional chemical stability are considered as a promising substrate to host a range of metallic nanoparticles [24]. Additionally, one-dimensional CNT can be converted into three-dimensional conductive networks through vacuum filtration to enable flow-through operations [25-27]. Such designs minimize the diffusional distance of reactants and expedited electrochemical reac-

* Corresponding authors.
E-mail addresses: ydjsp0107@ynu.edu.cn (S. Ji), yanbiaoliu@dhu.edu.cn (Y. Liu).

https://doi.org/10.1016/j.cclet.2024.110293
1001-8417/

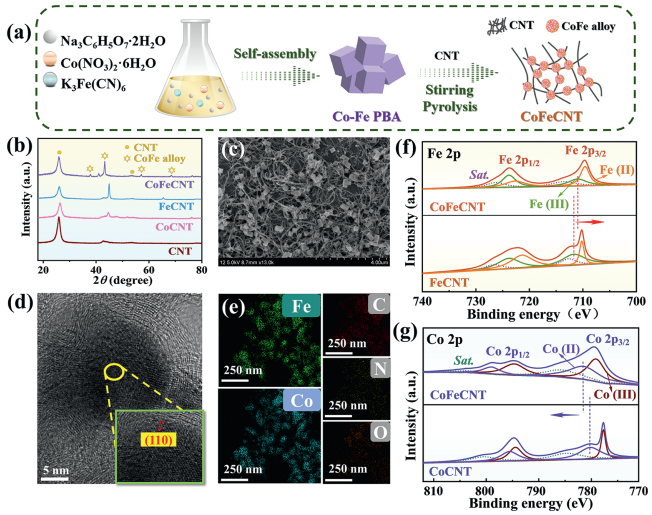

Fig. 1. (a) Schematic diagram displaying the preparation of the CoFeCNT. (b) Comparison of XRD patterns of CoFeCNT, CoCNT, FeCNT and CNT. (c) SEM and (d) TEM images of CoFeCNT. (e) EDS mapping image of CoFeCNT. The corresponding deconvoluted XPS spectra of (f) Fe 2p and (g) Co 2p.

tions, thereby bolstering both the destruction of pollutants and the anti-fouling performance of the reactive filter membrane [28,29].

Herein, we present a facile strategy to functionalize CoFe alloy nanoparticles on CNT (CoFeCNT) to electrocatalytically transform O_2 into $^1O_2$ *via* a 3-electron pathway in a flow-through configuration. The results show that the targeted production of $^1O_2$ is successfully attained during the electrocatalytic process through the incorporation of adjacent Co atoms at Fe active sites. The Co atoms effectively modulate the electronic structure of the resulting alloy nanoparticles, leading to a substantial enhancement in both catalytic performance and durability. Through a combination of electrochemical characterizations and experimental results, the alloying effects of CoFeCNT are shown to facilitates the donation of electrons from Co to Fe, which proves advantageous for the creation of $^1O_2$ *via* electron transfers from Co sites to $^*H_2O_2$. Furthermore, the system efficacy for purifying contaminated water is assessed using tetracycline (TC) as a representative organic contaminant. The essential process parameters are identified and fine-tuned to achieve optimal performance. This study offers valuable insights into the structure-performance correlation of metal-based alloy catalysts and the activation of molecular O_2 for the efficient elimination of organic micropollutants *via* the formation of $^1O_2$.

All chemicals and reagents were of analytical grade and used without further purification (Text S1 in Supporting information). The synthesis of the CoFeCNT nanohybrid filter started from the pyrolysis of CoFe-PBA. Details on the preparation of PBA precursor and material characterization are provided in Fig. S1 and Texts S2-S9 (Supporting information).

Fig. 1a elucidated the facile synthesis procedure of the CoFeCNT. Representative X-ray diffraction (XRD) patterns matched well the standard card (PDF #49–1568), confirming the successful fabrication of CoFeCNT with moderate crystallinity (Fig. 1b). Scanning electron microscopy (SEM) images showed that the CoFe alloy nanoparticles (diameter 200±10 nm) were randomly and homogeneously distributed on the interlaced CNT networks after the high-temperature calcination treatment (Fig. 1c). Transmission electron microscopy (TEM) was used to determine crystallinity of the CoFeCNT had a lattice spacing of 0.20 nm, indexed to the (110) facet of CoFe alloy [30], which matched the XRD results (Fig. 1d). The existence of Co and Fe in CoFeCNT was proven with energy dispersive X-ray spectroscopy (EDS) mapping of the CoFeCNT (Fig. 1e), in which the elements N, C, and O were homogeneously distributed throughout the structure. X-ray photoelectron spectroscopy (XPS) was employed to further investigate the elemental bonding status and the electronic interactions of Co and Fe. The Fe 2p XPS spectrum (Fig. 1f) showed that the binding energy of CoFeCNT was down-shifted compared to that of FeCNT, indicating a modification in the electron density of states, which could enhance the electrocatalytic activity and the adsorption of reaction intermediates [31]. In contrast, the peaks corresponding to the Co species in the XPS spectrum of CoFeCNT were shifted to a higher binding energy (Fig. 1g), indicating the transfer of charge between Fe and Co [32]. The XPS analysis revealed that charge transfer was caused by the reconstruction of electronic structure occurring with the CoFe alloying. This reconstruction could significantly affect the ORR performance of the CoFeCNT electrocatalyst [17].

The electrocatalytic ORR performance of the synthesized electrocatalysts toward O_2 activation was investigated first with cyclic voltammetry (CV). Fig. 2a showed a more positive ORR cathodic peak (0.72 V *vs.* RHE) corresponding to CoFeCNT in an O_2-saturated electrolyte (denoted as CoFeCNT/E/(O_2)), providing evidence of the significant enhancement of the material for catalyzing the ORR. To better understand the underlying mechanism of the evolution of O_2 molecules on the solid-liquid interface, a rotating ring-disk electrode (RRDE) measurement was conducted due to its advantages in elucidating the ORR behavior of electrocatalysts. Linear sweep voltammetry (LSV, Fig. 2b) curves of the as-synthesized electrocatalysts showed that the CoFeCNT electrocatalyst exhibited an evident positive onset potential (E_{onset} = 0.61 V *vs.* RHE) to its monometallic counterparts, revealing the synergistic effect of the bimetallic sites in terms of enhancing the activation of O_2. Another important characteristic of the electrocatalysts was the selectivity of the 3e$^-$ ORR relative to the more conventional 2e$^-$ or 4e$^-$ reduction of O_2 to H_2O_2 or H_2O. To better understand this selectivity, the average electron transfer number (n) was calculated from the disk and ring current density to further assess the 3e$^-$ ORR performance using different samples as cathode materials. As presented in Fig. 2c, both FeCNT and CoCNT provided a less favorable 3e$^-$ pathway, with n values calculated to be 3.6 and 2.4, respectively. For comparison, CoFeCNT had a much greater 3e$^-$ ORR activity with an n value of ~3.0 over a potential range of 0.1–0.6 V *vs.* RHE, revealing that the alloy effect effectively changed the reaction path of the ORR process [33]. A pivotal characteristic of 3e$^-$ ORR process is its capacity to function independently of H_2O_2 while effectively removing organic pollutants [34]. The yields of H_2O_2 in different fluidic systems were measured with UV–vis spectroscopy. As shown in Fig. S2 (Supporting information), the concentration of accumulated H_2O_2 in the FeCNT/E/(O_2) and CoCNT/E/(O_2) system within 90 min was 16.9 and 10.1 mmol h^{-1} m^{-2}, respectively. In contrast, a negligible amount of H_2O_2 was detected in the CoFeCNT/E/(O_2) system, indicating that the possibility of a fast one-electron transfer between $^*H_2O_2$ and Co sites, and there by implying the existence of the 3e$^-$ ORR.

In a typical ORR process, a multistep electron transfer pathway is involved, which can generate several intermediates, such as *O, *OH, and *OOH. To analyze the ORR process in this work, *in situ* Fourier-transform infrared (FTIR) spectroscopy was performed to recognize the stretching frequency corresponding to reaction intermediates formed during the 3e$^-$ ORR in the CoFeCNT/E/(O_2) system. The characteristic peaks at 1276 cm^{-1} and 1339 cm^{-1} emerged and intensified (Fig. 2d), which indicated the O–O stretching mode exhibited by $^*O_2$ on the CoFeCNT surface (aligning with the end-on (Pauling model) adsorption configuration) [15,35]. Also, the intensity of *OOH continued to increase appreciably, while the band associated with the *OOH bending vibration of *HOOH at 1353 cm^{-1} maintained a steady presence. This suggested a prevailing dissociative pathway, in which the strong attachment of *OOH

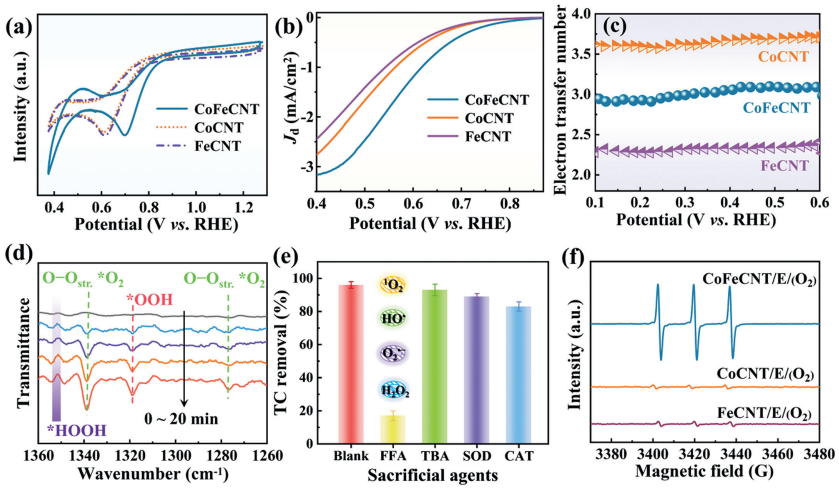

Fig. 2. (a) CV curves, (b) LSV curves, and (c) electron transfer number (*n*) in the RRDE measurements of CoCNT, FeCNT, and CoFeCNT electrodes. (d) FTIR spectra of the CoFeCNT fluidic electrode. (e) Comparison of the TC removal under different quenching conditions. (f) Spin-trapping EPR spectra for the detection of $^1O_2$ using TEMP as a trapping agent in different systems. Experimental conditions: $[TC]_0 = 0.02$ mmol/L, $[Na_2SO_4] = 50$ mmol/L, $pH_{initial} = 7$ and current density = 1 mA/cm^2.

to the electrode surface disrupted the O–O bond, potentially generating ROS [34].

To reveal the mechanism of catalytic behaviors in the CoFeCNT/E/(O_2) system, the generated ROS was first examined with conducting radical quenching experiments. The same concentration (50 mmol/L) of furfuryl alcohol (FFA, a scavenger for $^1O_2$), *tert*–butanol (TBA, a scavenger for •OH), superoxide dismutase (SOD, a scavenger for $O_2^{\bullet-}$) and catalase (a scavenger for H_2O_2) were introduced. The results confirmed that excessive amounts of FFA exerted a more pronounced inhibitory effects than TBA, underscoring the significance of $^1O_2$ as the predominant ROS (Fig. 2e). Additionally, a comparable inhibitory effect was observed in the presence of SOD and catalase, implying the potential involvement of $O_2^{\bullet-}$ and H_2O_2 in the degradation of pollutants, which likely stemmed from their function as intermediates for the generation of $^1O_2$.

Moreover, the direct observation of radicals within diverse systems is necessary to fully understand the underlying mechanism. Electron paramagnetic resonance (EPR) spectroscopy was utilized to differentiate different ROS by employing 5,5-dimethyl-1-pyrroline-*N*-oxide (DMPO) and 2,2,6,6-tetramethyl-4-piperidone (TEMP) as spin-trapping agents. Prominent signals for the TEMP-$^1O_2$ adduct (with a height ratio = 1:1:1) appeared in the CoFeCNT/E/(O_2) system, indicating the substantial production of $^1O_2$. Nevertheless, no discernible EPR signals corresponding to TEMP-$^1O_2$ adducts were detected in the O_2-free condition (Fig. S3 in Supporting information), implying that the generation of $^1O_2$ is specifically linked to the 3e$^-$ ORR process. A relatively subdued peak intensity of the TEMP-$^1O_2$ adduct occurred in both the FeCNT/E/(O_2) and CoCNT/E/(O_2) systems, possibly indicating the comparatively poor 3e$^-$ ORR activity of the FeCNT and CoCNT electrodes (Fig. 2f). In addition, there was a notable absence of signals associated with the DMPO-$O_2^{\bullet-}$ and DMPO-•OH adducts in the CoFeCNT/E/(O_2) system, again inferring that $^1O_2$ served as the predominant ROS (Fig. S4 in Supporting information).

On the basis of these results, a schematic illustration outlining the catalytic activation mechanism of CoFeCNT was developed, as depicted in Fig. 3. In the process of the electroactivation of molecular O_2, the O_2 was preferentially adhered "end-on" onto the Fe sites on the surface of CoFeCNT to form $^*O_2$, which was facilitated by the downward adjustment of the D-band center in the electronic structure of Fe, a modification brought about by the introduction of Co [33]. Subsequently, $^*O_2$ was efficiently transformed

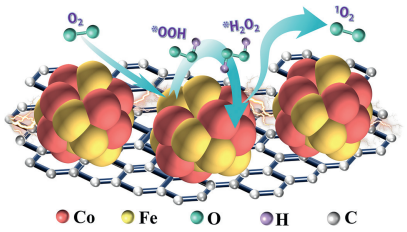

Fig. 3. Proposed electrocatalytic activation mechanism of molecular O_2 over the CoFeCNT filter.

into $^*H_2O_2$ *via* a swift two-step process involving single-electron transfers [20]. Since the alloy effect of CoFeCNT altered the intermetallic electronic structure and enhanced the adsorption affinity of the reactants and intermediates at the catalytic sites, the $^*H_2O_2$ swiftly produced $^1O_2$ on Co sites through a fast one-electron reduction pathway [23].

The swift escalation of antibiotic pollution in the environment poses a significant concern for human health. In contrast to other ROS, $^1O_2$ is believed to offer a new strategy for selective environmental remediation because it can preferably react with electron-rich moieties of organic molecules in complex water matrices and is less susceptible to interference from background materials. As a proof of concept, the antibiotic TC was selected as an example target contaminant to assess the electrocatalytic capabilities of the CoFeCNT filter. The TC degradation efficiency of the CoFeCNT/E/(O_2) system (96%) was 1.5 times and 1.2 times higher than that of FeCNT/E/(O_2) and CoCNT/E/(O_2) systems, respectively (Fig. 4a), being one of the most active catalysts *via* 3e$^-$ ORR. Moreover, only 30% of TC was degraded with CNT alone, which was possibly due to an electrochemical adsorption effect (Fig. S5 in Supporting information). Physical and electrochemical adsorption accounted for 24% and 43% of the TC removal, respectively (Fig. 4b), indicating that the TC degradation was overwhelmingly induced by electrocatalytic reaction with the CoFeCNT filter in the presence of O_2. In addition, the TC degradation in the CoFeCNT/E/(O_2) system significantly decreased without O_2 or current density, which was consistent with the electrochemical adsorption and physical adsorption process, respectively (Fig. 4c).

To examine the mineralization degree of TC, the change of total organic carbon (TOC) was evaluated during the degradation of TC. The CoFeCNT/E/(O_2) system not only showed complete TC removal

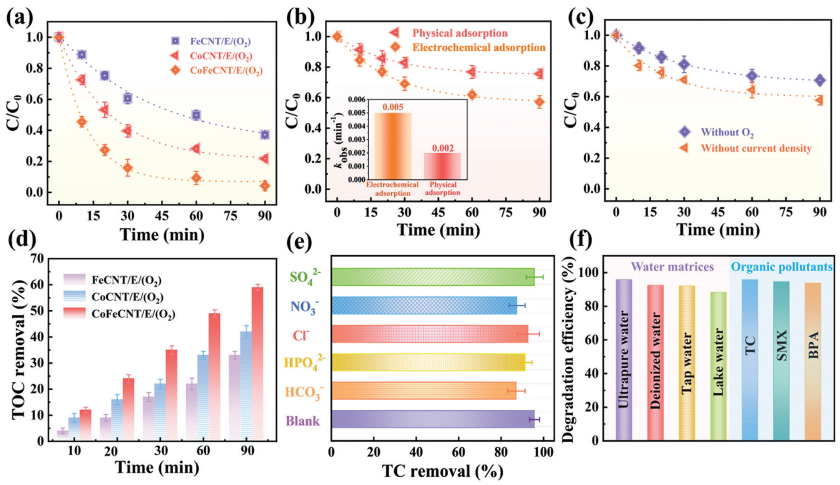

Fig. 4. (a) TC degradation in different systems. (b) Comparison of TC removal in different absorption processes. (c) The effect of O_2 and current density on the degradation of TC. (d) TOC removal in different systems. (e) Comparison of TC degradation in the presence of different coexisting anions. (f) The degradation efficiency of TC in CoFeCNT/E/(O_2) system in different sources of wastewater and pollutants. Experimental conditions: $[TC]_0 = 0.02$ mmol/L, $[Na_2SO_4] = 10$ mmol/L, $pH_{initial} = 7$, current density = 1 mA/cm^2 and flow rate = 4 mL/min.

but also a large removal of TOC (60%) within 90 min (Fig. 4d). The electrocatalytic efficacy of the CoFe/CNT/E/(O_2) filtration system was also compared to that of a conventional batch reactor (Fig. S6 in Supporting information). The resulting degradation efficiency in the flow-through system was significantly higher than that of traditional batch-fed reaction mode (*e.g.*, with a TC degradation of only 13%). The significant enhancement was due to the enhanced mass transport provided by forced convection in the flow-through configuration, while the batch reactor was limited by diffusion as its primary mass transfer pathway.

The nonradical mechanism governed by $^1O_2$ also demonstrated remarkable resistance to environmental disturbances. As illustrated in Fig. 4e, all common inorganic anions (*e.g.*, SO_4^{2-}, NO_3^-, Cl^-, HPO_4^-, HCO_3^-) posed a negligible impact on the degradation of TC in the CoFeCNT/E/(O_2) system. The CoFeCNT/E/(O_2) electrocatalytic system was also effective in activating O_2 over a broad pH range, underscoring the high pH tolerance of both the catalyst and $^1O_2$ (Fig. S7 in Supporting information). Significantly, the CoFeCNT/E/(O_2) system achieved consistent TC removal in a variety of water substrates (Fig. 4f, Table S1 in Supporting information), highlighting its promising prospects for practical utility. Attributed to the electron-capturing trait of $^1O_2$, the differential efficacy of the CoFeCNT in degrading electron-deficient micropollutants (carbamazepine, and 4-nitrophenol) compared to electron-rich contaminants (TC, bisphenol A and sulfamethoxazole), suggested a discernible degradation selectivity of the CoFeCNT/E/(O_2) system (Fig. S8 in Supporting information). Additional experiments were undertaken to investigate the impacts of catalyst dosage, flow rate and current density on the degradation of TC (Figs. S9 and S10 in Supporting information). Moreover, stability tests illustrated the outstanding reusability of CoFeCNT filter (Fig. S11 in Supporting information), demonstrating a consistent reactivity (>90%) and minimal leaching of Co or Fe (<0.01 mg/L) over a 48 h of successive runs, which is well below the standard of the World Health Organization (<0.3 mg/L).

In summary, an intensified and sustainable strategy was proposed to fabricate fluidic CoFeCNT alloy electrodes for selectively electroactivating the reduction of O_2 to $^1O_2$, and the viability was validated with both proof-of-concept investigations and practical applications in remediation efforts. The alloying of Co with Fe facilitated the electron donation from Co to Fe, which generated an ample supply of positively charged Co atoms that served as highly efficient sites for adsorbing H_2O_2 during the 3e$^-$ ORR process. Simultaneously, the redistribution of charges *via* the cohesive Co–Fe bonds boosted the activation of $^*H_2O_2$, ultimately leading to the creation of $^1O_2$. The exceptional system efficacy was sustained in complicated water matrices and was extended to various electron-rich micropollutants. This work sheds light on the mechanisms involved in activating molecular oxygen using transition metal oxides and presents a universal design framework for electrocatalysts, enhancing the effectiveness of current high-performance methods for the electrocatalytic production of $^1O_2$.

Declaration of competing interest

The authors declare that they have no known competing financial interests or personal relationships that could have appeared to influence the work reported in this paper.

CRediT authorship contribution statement

Shengtao Jiang: Writing – review & editing, Resources, Investigation, Funding acquisition, Conceptualization. **Mengjiao Xie:** Writing – original draft, Methodology, Investigation, Data curation. **Limin Jin:** Supervision, Methodology. **Yifan Ren:** Software, Methodology. **Wentian Zheng:** Supervision, Methodology. **Siping Ji:** Supervision, Investigation. **Yanbiao Liu:** Writing – review & editing, Supervision, Investigation, Funding acquisition.

Acknowledgments

This work was supported by the Natural Science Foundation of Shanghai (No. 23ZR1401300) and the National Natural Science Foundation of China (No. 52170068).

Supplementary materials

Supplementary material associated with this article can be found, in the online version, at doi:10.1016/j.cclet.2024.110293.

References

[1] F. Sun, X. Yang, F. Shao, et al., Chin. Chem. Lett. 34 (2023) 108563.
[2] D. Guo, S. Jiang, L. Jin, et al., J. Mater. Chem. A 10 (2022) 15981–15989.
[3] L. Jin, S. You, N. Ren, Y. Liu, Fundam. Res. 3 (2022) 770–776.
[4] D. Guo, S. You, F. Li, Y. Liu, Chin. Chem. Lett. 33 (2022) 1–10.
[5] F. Xiao, Z. Wang, J. Fan, et al., Angew. Chem. Int. Ed. 60 (2021) 10375–10383.
[6] S. Zhu, X. Li, J. Kang, et al., Environ. Sci. Technol. 53 (2019) 307–315.

[7] Y. Zhao, M. Sun, X. Wang, et al., Nat. Commun. 11 (2020) 6228.
[8] Z. Li, Y. Sun, Y. Yang, et al., Environ. Res. 183 (2020) 109156.
[9] G. Bi, R. Ding, J. Song, et al., Angew. Chem. Int. Ed. 63 (2024) e202401551.
[10] Q. Yi, J. Ji, B. Shen, et al., Environ. Sci. Technol. 53 (2019) 9725–9733.
[11] Y. Zhao, M. Sun, Y. Zhao, et al., Water Res. 225 (2022) 119140.
[12] L. Zhou, Y. Liu, H. Shi, et al., Water Res. 250 (2024) 121075.
[13] S. Mondal, D. Bagchi, M. Riyaz, et al., J. Am. Chem. Soc. 144 (2022) 11859–11869.
[14] H. Li, S. Kelly, D. Guevarra, et al., Nat. Catal. 4 (2021) 463–468.
[15] H. Gu, X. Liu, X. Liu, et al., Nat. Commun. 12 (2021) 4146.
[16] Z. Feng, M. Chen, Q. Yang, et al., Environ. Sci. Technol. 57 (2023) 17123–17131.
[17] G. Zhu, H. Yang, Y. Jiang, et al., Adv. Sci. 9 (2022) 2200394.
[18] Y. Li, Y. Feng, L. Li, et al., J. Alloys Compd. 823 (2020) 153892.
[19] X. Cheng, Y. Wang, Y. Lu, et al., Appl. Catal. B 306 (2022) 121112.
[20] S. Cheng, Y. Liu, H. Zheng, et al., Sep. Purif. Technol. 325 (2023) 124545.
[21] L. Xu, L. Duan, Y. Pan, et al., Sep. Purif. Technol. 303 (2022) 122137.
[22] T. Zhang, Y. Wang, X. Li, et al., Chin. Chem. Lett. 34 (2023) 107596.
[23] J. Xie, L. Zhong, X. Yang, et al., Chin. Chem. Lett. 35 (2024) 108472.
[24] Y. Liu, F. Liu, N. Ding, et al., Chin. Chem. Lett. 31 (2020) 2539–2548.
[25] L. Jin, S. You, N. Ren, et al., Environ. Sci. Technol. 56 (2022) 11750–11759.
[26] D. Guo, Y. Liu, H. Ji, et al., Environ. Sci. Technol. 55 (2021) 4045–4053.
[27] L. Jin, X. Duan, M. Sun, et al., ACS Nano 17 (2023) 12875–12883.
[28] M. Sun, X. Wang, L.R. Winter, et al., ACS ES&T Engg. 1 (2021) 725–752.
[29] Y. Zhao, M. Sun, L.R. Winter, et al., Environ. Sci. Technol. 56 (2022) 3832–3835.
[30] X. Zhu, T. Jin, C. Tian, et al., Adv. Mater. 29 (2017) 1704091.
[31] Q. Shi, Q. Liu, Y. Ma, et al., Adv. Energy Mater. 10 (2020) 1903854.
[32] F. Meng, H. Zhong, D. Bao, et al., J. Am. Chem. Soc. 138 (2016) 10226–10231.
[33] H. Luo, S. Li, Z. Wu, et al., Adv. Funct. Mater. 34 (2024) 2403838.
[34] L. Xie, P. Wang, W. Zheng, et al., Proc. Natl. Acad. Sci. U. S. A. 120 (2023) e2307989120.
[35] L. Xie, P. Wang, Y. Li, et al., Nat. Commun. 13 (2022) 5560.